

# ROBUST ESTIMATION OF MAXIMUM TIRE-ROAD FRICTION COEFFICIENT CONSIDERING ROAD SURFACE IRREGULARITY

K. HAN, Y. HWANG, E. LEE and S. CHOI\*

School of Mechanical, Aerospace & System Engineering, KAIST, Daejeon 34141, Korea

(Received 27 March 2015; Revised 30 June 2015; Accepted 9 November 2015)

**ABSTRACT**—An accurate estimation of the maximum tire-road friction coefficient may provide higher performance in a vehicle active safety control system. Unfortunately, real-time tire-road friction coefficient estimation is costly and necessitates additional sensors that must be installed and maintained at all times. This paper proposes an advanced longitudinal tire-road friction coefficient estimation method that is capable of considering irregular road surfaces. The proposed algorithm uses a stiffness based estimation method, however, unlike previous studies, improvements were made by suggesting a third order model to solve problems related to nonlinear mu-slip curve. To attain the tire-road friction coefficient, real-time normalized force is obtained from the force estimator as exerted from the tire in the low slip region using the recursive least squares method. The decisive aspect of using the suggested algorithm lies in its low cost and versatility. It can be used under irregular road conditions due to its capability of easily obtaining wheel speed and acceleration values from production cars. The newly improved algorithm has been verified to computer simulations as well as compact size cars on dry asphalt conditions.

**KEY WORDS** : Tire-road friction coefficient, Vehicle safety control system, Wheel dynamics, Unknown input observer, Suspension dynamics, Mu-slip curve

## NOMENCLATURE

$F$	: tire force, N
$\lambda_x$	: longitudinal tire slip ratio, –
$V$	: velocity, km/h
$T_o$	: output shaft torque, Nm
$m_s, m_u$	: sprung/unsprung mass, kg
$h$	: height of the mass center, m
$\ddot{x}_{cg}$	: longitudinal acceleration, m/s <sup>2</sup>
$l_{f,r}$	: distance center to front and rear wheels, m
$z_s$	: normal position at the sprung mass, m
$z_u$	: normal position at the un-sprung mass, m
$z_r$	: normal position at the road, m
$b_s$	: damping constant of suspension, Ns/m
$k_s$	: spring constant of suspension, N/m
$S$	: stiffness, –
$K(t)$	: update gain, –
$P(t)$	: error covariance, –
$\lambda$	: forgetting factor, –
$\varepsilon_{s,e}$	: curve fitting trigger/end signal, –

## SUBSCRIPTS

$x, y, z$	: direction of vehicle longitudinal/lateral/vertical
$\omega$	: wheel
$m$	: measured value

---

\*Corresponding author. e-mail: sbchoi@kaist.ac.kr

## 1. INTRODUCTION

Recently, demands to implement Anti-lock Braking System (ABS), Electronic Stability Program (ESP), and Traction Control System (TCS) have been on the rise (Choi, 2008; Nam *et al.*, 2010; Choi and Choi (2014); Yoon *et al.*, 2009; Rajamani, 2011; Hori *et al.*, 1998; Lian *et al.*, 2015; Kim *et al.*, 2015). However, aforementioned systems are useless if individual tires on the vehicle cannot be fully controlled. Thus, accurate measurements of individual tire forces are needed for control of the advanced security functions. There is a close relationship between the force exerted from a tire and surface friction coefficient, for example, the tire-road friction coefficient allows for the estimation of maximum traction force as well as braking force. However, obtaining real-time values of surface friction coefficient from a sensor is difficult due to high cost, lack of technology, and high maintenance. Therefore, an indirect method of obtaining tire-road friction coefficient is needed. The following approaches are from various published studies on the aforementioned methods.

First is the vision based estimation method (Holzmann *et al.*, 2006, Sato *et al.*, 2007). This is an evaluation of the road surface through a sensor without taking any physical excitation into consideration, including braking or accelerative force. This method allows the friction coefficient to be measured in real-time but highly depends on the quality of the sensor. While the expanded use of such a sensor will

create a competitive market and ultimately lower its price, nonetheless, the price of the sensor must be taken into consideration.

The second method, known as the wheel motion based estimation, is another approach that collects speed, wheel steering, traction and braking force from the controller (Gustafsson, 1998; Ito *et al.*, 1995). These values are easily obtained in production cars and therefore do not necessitate any additional sensors. However, these standard built-in sensors include measurement errors, and thus must be enhanced for performance degradation estimation due to those errors.

The third method utilizes additional sensors such as Global Positioning System (GPS) or 6D-IMU, also known as the vehicle dynamic based estimation method (Choi *et al.*, 2013; Cho *et al.*, 2010; Hahn *et al.*, 2002; Ahn *et al.*, 2013; Sierra *et al.*, 2006); a method taking lateral dynamics into consideration. A tire-road friction coefficient estimator in combination with longitudinal/latitudinal dynamics can be used in the Electronic Stability Program (ESP). Lastly, in this paper, a stiffness based estimation method with longitudinal dynamics was employed (Gustafsson, 1997; Wang *et al.*, 2004; Lee *et al.*, 2004; Rajamani *et al.*, 2012; Muller *et al.*, 2003; Ray, 1997). It is an extension of the basic wheel motion estimation method. The tire-road friction coefficient is proportional to tire slip in the lower range of the mu-slip curve. However, such a calculation method is not used by the auto industries because the stiffness based estimation innately has the possibility of over/under estimation. Therefore, in this paper, a stiffness based estimation method is proposed with improvements for obtaining tire-road friction coefficient on the irregular road surface.

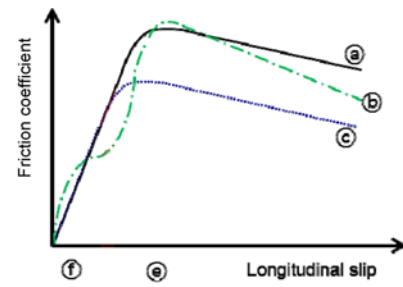
The main differences between this study and others preceding it are the implementation of the third order model to reduce the amount of calculation, and the use of an algorithm for irregular surfaces, respectively. The third order model of mu-slip curve was estimated using the Linearized Recursive Least Square (LRLS) method, and the software, Carsim, was used via simulation and on dry asphalt surface with a compact size car.

The paper is organized in the following way. Section 2 discusses the estimation strategy and its advantages and disadvantages. Section 3 discusses the suggested algorithm and Section 4 shows the results from various simulations and experiments. Finally, Section 5 concludes the paper.

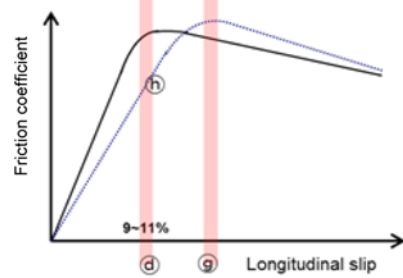
## 2. ESTIMATION STRATEGY OVERVIEW

### 2.1. Practical Issues on Stiffness based Estimation of Road Friction Coefficient

Before discussing the advanced tire-road friction coefficient, the current or published estimation method and its flaws are analysed below. First, an assumption must be made to have an ideal mu-slip curve with linear qualities in the low slip range. However, a non-linear curve occurs within the



(a) Irregular mu slip curve



(b) Variable slip region generating maximum tire force

Figure 1. Practical issues on stiffness based tire-road friction coefficient estimation method.

experimental settings as shown in Figure 1 (line (b)). Vibration can be observed on irregular surfaces with the use of current estimation methods due to changes of stiffness, resulting in a divergence of estimation value. In addition to this defect, line (a) and line (c) of Figure 1 are representations of an ideal linear mu-slip curve before reaching saturation, however, the maximum tire-road friction coefficients are different. Second, the assumption must be made that the maximum tire force in a given slip range is between 9 ~ 11%. In other words, peak slip region is fixed in the conventional tire model. However, this value cannot be fixed because the design of the tire and various surface conditions produce different forces from the tire under various slip ranges. Such fixed values will underestimate the friction coefficient curve as seen in Figure 1 (b). These problems have been recognized by automakers and remain a challenging to be solved.

### 2.2. Estimation Approach

The following normalized force can be used only if the longitudinal dynamics are considered in the tire-road friction coefficient.

$$\mu = F_{\text{nor}} = \frac{\sqrt{F_x^2 + F_y^2}}{F_z} \approx \frac{F_x}{F_z} \quad (1)$$

The force from a longitudinal and lateral tire is indirectly estimated from the wheel speed or 6-DOF sensors. Furthermore, any longitudinal dynamics including drive/brake/torque are measured from various sensors in production cars. The value for the normalized force is

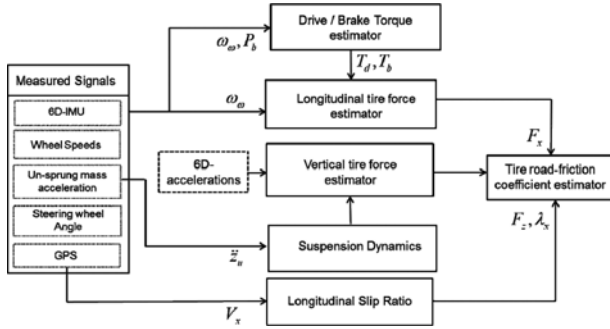


Figure 2. Block diagram of proposed tire-road friction coefficient estimator.

obtained with respect to slip, based on the estimated lateral/longitudinal dynamic. The slip is defined as follows.

$$\lambda_x = \frac{V_\omega - V_x}{V_\omega} : \text{acceleration} \quad (2)$$

$$\lambda_x = \frac{V_x - V_\omega}{V_x} : \text{deceleration} \quad (3)$$

This paper proposes a third order model (4) to represent surface irregularity and the starting point of saturation. The suggested estimation diagram is shown in Figure 2. More detailed overall-estimation is discussed in Section 3.

$$F_{\text{nor}} \approx \sum_{i=0}^2 p_i \lambda_x^{i+1} \quad (4)$$

where  $p_i$  is the unknown parameter.

### 3. MAXIMUM TIRE-ROAD FRICTION COEFFICIENT ESTIMATION

The estimation of tire force must be received from a functioning sensor as represented in Figure 2. There are many studies (Choi *et al.*, 2013; Cho *et al.*, 2010; Choi and Choi (2013); Rajamani *et al.*, 2012; Wang *et al.*, 2004) regarding tire force estimation, and several have focused solely on the lateral tire force for control of lateral movement of vehicle. However, this paper focuses on longitudinal movement and the force of a vertical tire.

#### 3.1. Longitudinal Tire Force Estimation

The estimation of longitudinal tire force is obtained from a car with ABS using the accessible signal of wheel speed. The equation for wheel dynamics is as follows.

$$\dot{\omega}_\omega = \frac{1}{J_\omega} (R_c F_x + T_d - T_b - R_c F_{rr}) \quad (5)$$

where  $\omega_\omega$  is the wheel speed at the individual wheel,  $R_c$  the effective wheel radius,  $T_d$  and  $T_b$  are drive and brake torque at the wheel and  $F_{rr}$  the rolling resistance.

Unknown Input Observer (UIO) (Chen and Saif, 2006; Han *et al.*, 2014) can be implemented as seen in Equation (7), assuming the differential value of longitudinal tire

force is negligible in Equation (5).

First, the state space representation can be shown in terms of wheel dynamics.

$$\begin{bmatrix} \dot{\hat{\omega}}_\omega \\ \dot{\hat{F}}_x \end{bmatrix} = \begin{bmatrix} 0 & R_c \\ J_\omega & 0 \end{bmatrix} \begin{bmatrix} \hat{\omega}_\omega \\ \hat{F}_x \end{bmatrix} + \begin{bmatrix} 1 \\ 0 \end{bmatrix} T_d - \begin{bmatrix} T_b + R_c F_{rr} \\ 0 \end{bmatrix} \quad (6)$$

Now, Equation (6) becomes the wheel speed feedback signal for UIO application.

$$\begin{bmatrix} \dot{\hat{\omega}}_\omega \\ \dot{\hat{F}}_x \end{bmatrix} = \begin{bmatrix} 0 & R_c \\ J_\omega & 0 \end{bmatrix} \begin{bmatrix} \hat{\omega}_\omega \\ \hat{F}_x \end{bmatrix} + \begin{bmatrix} 1 \\ 0 \end{bmatrix} \hat{T}_d - \begin{bmatrix} \hat{T}_b + R_c \hat{F}_{rr} \\ 0 \end{bmatrix} + \dots \\ \dots + \begin{bmatrix} l_1 \\ -l_2 \end{bmatrix} (\omega_{\omega,m} - \hat{\omega}_\omega) \quad (7)$$

where  $l_1$  and  $l_2$  are observer gain,  $\hat{\bullet}$  is the estimated state and  $\omega_m$  the measured wheel speed at the individual wheels.

Next, drive/brake torque values are obtained by using the Luenberger type observer (Han *et al.*, 2014).

$$J_v \dot{\hat{\omega}}_\omega = \hat{T}_\omega - \hat{T}_{L,\text{model}} + l(\omega_{\omega,m} - \hat{\omega}_\omega) \\ \hat{T}_{L,\text{model}} = R_c \left\{ \begin{array}{l} m_v g \sin(\theta_{\text{road}}) + K_{rr} m_v g \cos(\theta_{\text{road}}) \\ \text{road inclination} \quad \text{rolling resistance} \\ \dots + \frac{1}{2} \rho v_x^2 C_d A_f \\ \text{aerodynamic drag} \end{array} \right\} \quad (8)$$

where  $T_\omega$  is the output shaft torque from transmission which is distributed to driving wheel evenly,  $J$ , the total inertia of vehicle,  $T_{L,\text{model}}$  the vehicle external load,  $l$  the observer gain,  $m_v$  mass of vehicle,  $g$  the gravity acceleration constant,  $\theta_{\text{road}}$  the slope of road,  $\rho$  the air density,  $v_x$  the vehicle speed,  $C_d$  the aerodynamic drag coefficient and  $A_f$  the frontal area of the vehicle.

Equation (8) shows the output shaft torque in terms of momentum of driving load where the estimation of driving load becomes more accurate by using wheel speed estimation as the feedback signal. An accurate driving load estimation will prevent over/under estimation of the shaft torque output. The shaft torque output is then used to measure the force exerted from the tire in longitudinal movement during acceleration.

Below is the braking torque estimation. Estimation of the braking torque comes from pressure of the master cylinder while assuming the hydraulic brake is treated as an ideal state (Munson *et al.*, 1990) is shown below.

$$\hat{T}_b = K_f P_{mc} - \tau \frac{d\hat{T}_b}{dt} \quad (9)$$

where  $K_f$  is the brake gain,  $P_{mc}$  the master cylinder pressure and  $\tau$  the time constant.

The stability of the suggested algorithm is proven as follows. If the drive/brake torque values of the longitudinal tire force is adequate, subtracting Equation (6) from error dynamics Equation (7) will result in the following.

$$J_o \dot{\tilde{\omega}}_o = R_c \tilde{F}_x - l_1 \tilde{\omega}_o \quad (10)$$

Differentiation of Equation (10) in terms of time and the addition of Equation (7) will result in Equation (11)

$$\begin{aligned} J_o \ddot{\tilde{\omega}}_o + l_1 \dot{\tilde{\omega}}_o - R_c \dot{\tilde{F}}_x &= 0 \\ J_o \ddot{\tilde{\omega}}_o + l_1 \dot{\tilde{\omega}}_o + l_2 R_c \tilde{\omega}_o &= 0 \end{aligned} \quad (11)$$

When using the positive gain values the closed loop error dynamics converges to 0.

### 3.2. Vertical Tire Force Estimation

The estimator for vertical tire force proposed in this paper has been designed to incorporate all the physical motions of cars with 6-DOF. The tire force of a quarter car (Figure 3) model with longitudinal load transfer (Rajamani *et al.*, 2012; Wang *et al.*, 2004) is as follows.

$$\begin{aligned} \hat{F}_{z,FL} &= (m_{s,FL} + m_{u,FL})g - \frac{(m_s + m_u)\ddot{x}_{cg}h}{2(l_f + l_r)} \\ \hat{F}_{z,FR} &= (m_{s,FR} + m_{u,FR})g - \frac{(m_s + m_u)\ddot{x}_{cg}h}{2(l_f + l_r)} \\ \hat{F}_{z,RL} &= (m_{s,RL} + m_{u,RL})g - \frac{(m_s + m_u)\ddot{x}_{cg}h}{2(l_f + l_r)} \\ \hat{F}_{z,RR} &= (m_{s,RR} + m_{u,RR})g - \frac{(m_s + m_u)\ddot{x}_{cg}h}{2(l_f + l_r)} \end{aligned} \quad (12)$$

Only longitudinal load transfer was reflected assuming the overall mass of the quarter car model in Equation (12) is equally distributed. However, the vertical tire force

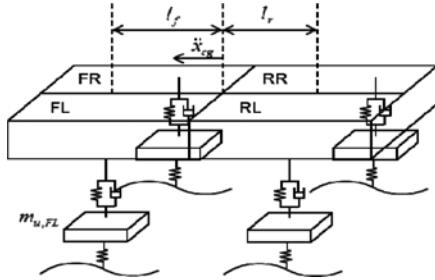


Figure 3. Quarter car model.

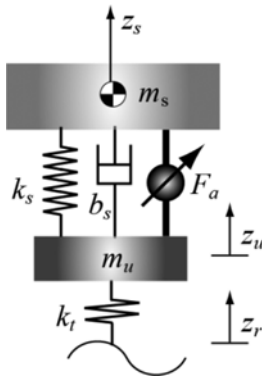


Figure 4. Suspension dynamic.

estimator, like that of Equation (12), does not include effect of suspension dynamics, hence, this paper has included the vertical tire force estimator with the effects of the suspension phenomena.

Both sprung and unsprung masses are interconnected like that of the spring-damper system as seen in Figure 4. Once the vertical movement of a car is considered, suspension dynamics equations can be written as Equations (13) and (14).

$$m_s \ddot{z}_s = -b_s(\dot{z}_s - \dot{z}_u) - k_s(z_s - z_u) \quad (13)$$

$$m_u \ddot{z}_u = -b_s(\dot{z}_u - \dot{z}_s) - k_s(z_u - z_s) - k_t(z_u - z_r) \quad (14)$$

Additional effects of suspension in Equation (14) will give Equation (15) and adding the latter to Equation (12) will allow for surface disturbance to obtain vertical tire force.

$$F_{z,dyn} = k_t(z_u - z_r) = -b_s(\dot{z}_u - \dot{z}_s) - k_s(z_u - z_s) - m_u \ddot{z}_u \quad (15)$$

Equation (15) needs additional sensors that can detect properties like rattle space ( $z_u - z_r$ ) and relative velocity ( $\dot{z}_u - \dot{z}_s$ ). However, the high cost of instruments is an issue for use in production cars.

The suggested method shown in Kim *et al.* (2013) will be modified and used to circumvent the problem. Adding Equations (13) and (14) will give Equation (16).

$$F_{z,dyn} = m_s \ddot{z}_s + m_u \ddot{z}_u \quad (16)$$

Equation (16) needs both the sprung and unsprung mass vertical accelerator ( $\ddot{z}_s, \ddot{z}_u$ ) factor. In order to get the unsprung mass vertical accelerator factors, each wheel will be attached with cost-effective accelerometers. However, it is difficult to get the sprung mass accelerator factors solely through sensors. Therefore, it will be indirectly measured using Equation (17). Each of the sprung mass accelerator factors can be calculated by integrating roll, pitch, and heave from the center of the mass. 6D-IMU will provide these values : longitudinal / lateral / heave accelerations ( $a_x, a_y, a_z$ ), yaw / pitch / roll accelerations ( $\ddot{\psi}, \ddot{\theta}, \ddot{\phi}$ ). All values from the quarter car model can be combined to give the following.

$$\begin{aligned} \ddot{z}_{s,FL} &= \ddot{z}_{cg} - l_f \ddot{\theta} - \frac{l_w}{2} \ddot{\phi} \\ \ddot{z}_{s,FR} &= \ddot{z}_{cg} - l_f \ddot{\theta} + \frac{l_w}{2} \ddot{\phi} \\ \ddot{z}_{s,RL} &= \ddot{z}_{cg} + l_r \ddot{\theta} - \frac{l_w}{2} \ddot{\phi} \\ \ddot{z}_{s,RR} &= \ddot{z}_{cg} + l_r \ddot{\theta} + \frac{l_w}{2} \ddot{\phi} \end{aligned} \quad (17)$$

Although this paper has only taken the longitudinal dynamics into consideration, the roll acceleration in Equation (17) was included due to a slight steering angle which was observed within the experimental data from Section 4. Ultimately, combining Equations (17) and (12) will give the total individual vertical tire force in the quarter car model as follows.

$$\begin{aligned}
 \hat{F}_{z,FL} &= (m_{s,FL} + m_{u,FL})g - \frac{(m_s + m_u)\ddot{x}_{cg}h}{2(l_f + l_r)} + m_s\ddot{z}_{s,FL} + m_u\ddot{z}_u \\
 \hat{F}_{z,FR} &= (m_{s,FR} + m_{u,FR})g - \frac{(m_s + m_u)\ddot{x}_{cg}h}{2(l_f + l_r)} - m_s\ddot{z}_{s,FR} - m_u\ddot{z}_u \\
 \hat{F}_{z,RL} &= (m_{s,RL} + m_{u,RL})g - \frac{(m_s + m_u)\ddot{x}_{cg}h}{2(l_f + l_r)} + m_s\ddot{z}_{s,RL} + m_u\ddot{z}_u \\
 \hat{F}_{z,RR} &= (m_{s,RR} + m_{u,RR})g - \frac{(m_s + m_u)\ddot{x}_{cg}h}{2(l_f + l_r)} - m_s\ddot{z}_{s,RR} - m_u\ddot{z}_u
 \end{aligned} \quad (18)$$

3.3. Stiffness based Road Friction Coefficient Estimation  
 Prior to introducing the specifics of the estimation methods within this paper, a background in stiffness, on which this paper is based on, will be discussed. It is used for comparing the linear properties between force and slip ranges in the low slip range as seen in Equation (19).

$$\hat{\mu}_x = \hat{F}_{nor} = \frac{\hat{F}_x}{\hat{F}_z} = S \cdot \hat{\lambda}_x \quad (19)$$

We assume that estimation of stiffness bases has unique properties in the low slip-range for each different road surface (Wang *et al.*, 2004). These specific stiffness properties can be obtained by using the Recursive Least Square (RLS) method as follows.

$$\begin{aligned}
 \hat{S}(t) &= \hat{S}(t-1) + K(t) \left\{ \frac{\hat{F}_x(t)}{\hat{F}_z(t)} - \hat{S}(t-1)\lambda_x(t) \right\} \\
 K(t) &= \frac{P(t-1)\lambda_x(t)}{\lambda + P(t-1)\lambda_x^2(t)} \\
 P(t) &= \frac{1}{\lambda} \left\{ P(t-1) - \frac{P^2(t-1)\lambda_x(t)}{\lambda + P(t-1)\lambda_x^2(t)} \right\}
 \end{aligned} \quad (20)$$

where  $K(t)$  is the update gain,  $P(t)$  the error covariance and  $\lambda$  the forgetting factor.

The use of the forgetting factor (Paleologu *et al.*, 2008) in the overall process is for weighting more importance to modern data rather than those of outdated data, which cannot be expressed concretely. In other words, the smaller the  $\lambda$  the lower the influence of outdated data, while it may react sensitively to modern data. Obtaining innate stiffness of surface can be calculated via the RLS method, which in turn can be used to estimate the maximum tire-road friction coefficient.

### 3.4. Advanced Estimation Method

As mentioned in Section 2, the given basic stiffness estimation had a few problems and an advanced tire-road friction coefficient estimation method was proposed. This method not only uses current stiffness bases but suggests third order model real-time curve fitting.

The suggested third order model, as seen in Figure 5, will pass through the point of origin and inflection point. The properties of the dotted lines are dependent on the normalized tire forces (dots on low slip region). In other words, third order polynomial model, which concentrates on the low slip region curve shape, is obtained according to

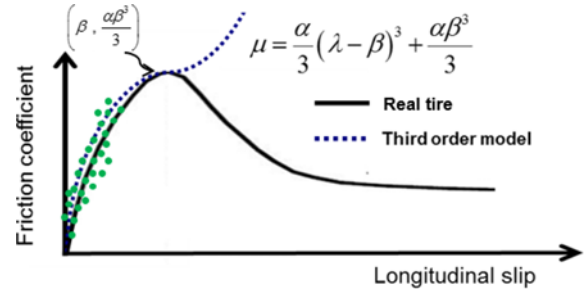


Figure 5. Third order polynomial model for real-time curve fitting.

the real tire data to reflect the irregular road surfaces, which can be occasionally shown in the real world. In Figure 5, the suggested model has inflection point that is identical to start point of tire force saturation. The curve shape beyond the inflection point is not considered in this study because accurate curve fitting of mu-slip curve is beyond the scope of this paper and the main concern of this study is adaptive shaping of mu-slip curve on the low slip region based on real tire data.

The differentiation of the third order model is as follows.

$$\mu'_x = f'(\lambda_x) = \alpha(\lambda_x - \beta)^2 \quad (21)$$

Equation (21) is important in two different ways: it includes two unknown parameters that are crucial in forming irregular surface phenomena. The integral of Equation (21) will give a more complete form of the third order model Equation (22).

$$f(\lambda_x) = \frac{\alpha}{3} (\lambda_x - \beta)^3 + \mu_{max} \quad (22)$$

Because the third order model passes through the point of origin, its maximum tire-road friction coefficient is at the inflection point with the value of  $\alpha\beta^3/3$ .

Finally, the third order model is summed up as;

$$F_{nor} = \sum_{i=0}^2 p_i \lambda_x^{i+1} = \frac{\alpha}{3} (\lambda_x - \beta)^3 + \frac{\alpha\beta^3}{3} \quad (23)$$

The maximum tire-road friction coefficient is obtained by measuring the unknown parameter value of the third order model using the RLS method. The proposed third order model includes nonlinear properties, thus Linearized Recursive Least Square (LRLS) in conjunction with Equation (24) must be employed for parameter adaptation.

$$\begin{aligned}
 y(t) &= F_{nor}, \theta(t) = [\alpha \quad \beta]^T \\
 y(t) &= f(\theta, t) = \frac{\alpha}{3} (\lambda - \beta)^3 + \frac{\alpha\beta^3}{3} \\
 F^T(t) &= \frac{\partial f(\theta, t)}{\partial \theta} \Big|_{\theta=\hat{\theta}(t-1)} = \left[ \frac{\partial f(\theta, t)}{\partial \alpha} \quad \frac{\partial f(\theta, t)}{\partial \beta} \right]
 \end{aligned} \quad (24)$$

In Equation (24), the third order model is linearized for every sample time and implemented to the Recursive Least Square (RLS) method like that of Equation (25).

$$\begin{aligned}
y(t) &= F^T(t)\theta(t) \\
\hat{\theta}(t) &= \hat{\theta}(t-1) + K(t) \left[ y(t) - \hat{f}(\theta, t) \right] \\
P(t) &= \frac{1}{\lambda} \left[ P(t-1) - \frac{P(t-1)F(t)F^T(t)P(t-1)}{\lambda + F^T(t)P(t-1)F(t)} \right] \\
K(t) &= \frac{P(t-1)F(t)}{\lambda + F^T(t)P(t-1)F(t)}
\end{aligned} \quad (25)$$

The proposed algorithm and its advantages are summarized below.

First, recognizing the nonlinear properties of the third order model for irregular surfaces was taken into consideration. As such, it is now possible, as seen in Figure 1, to differentiate various tire-road friction coefficients even despite equal initial stiffness, which cannot be covered by previous works. Moreover, the simplicity of this model allows for less calculation effort in comparison to the conventional tire model such as magic formula (Pacejka, 2005) or the brush tire model (Choi *et al.*, 2013).

Secondly, the unknown parameter  $\beta$  represents the starting point of saturation, and unlike previous studies where the point of saturation was fixed, this paper has made  $\beta$  a flexible value and estimated it through the RLS method. Therefore, the proposed algorithm is allowed to express irregular road surfaces and prevent both over/under estimated values as shown in Figure 1 (b).

Thirdly, real-time observation of the third order model curve fitting allows for calculation of the maximum tire-road friction coefficient before the friction coefficient reaches its point of saturation. Because tire-road friction limit estimation is meaningful when it is predicted in a stable region where tire force is proportional to longitudinal slip. In other words, early detection of maximum tire friction limit is crucial in the vehicle control research area.

Finally, the robustness of the algorithm is obtained by using the previous stiffness based method results as a triggering signal to the proposed algorithm. This will be discussed in detail in the following section.

### 3.5. Normalized Stiffness Factor

This section proposes a normalized stiffness factor using the previous stiffness base estimation method. The RLS algorithm is an estimation method to lower error covariance by repeating estimation process repeatedly. During repeated trials, unnecessary data introduces inaccurate information that cannot properly express the overall curve phenomena. Most of the inaccuracies are shown within the 1% ~ 2% low slip range. That is why it is imperative to distinguish the effectiveness of values obtained from the algorithm, which can become trigger/end signals. This proposed algorithm will maintain robustness via normalized stiffness factor on various irregular surfaces as shown below. Most road surfaces show linear properties in the low slip range but quickly saturate after a certain point. In other words, the point where the linearity of the mu-slip curve becomes saturated is the point where curving fitting starts. The

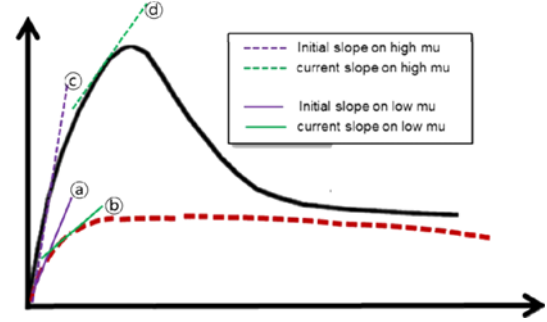


Figure 6. Normalized stiffness factor.

discussion below shows how normalizing estimation of stiffness can be used for the aforementioned algorithm.

$$\varepsilon_s \leq \frac{\hat{S}_e(t)}{\hat{S}_i(t)} \leq \varepsilon_e \quad (26)$$

where  $\hat{S}_e, \hat{S}_i$  are the estimated current stiffness, estimated initial stiffness and  $\varepsilon_s, \varepsilon_e$  are the curve fitting trigger signal and curve fitting end signal.

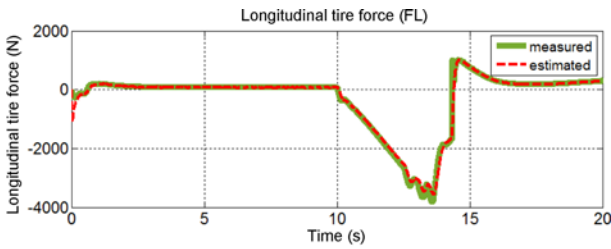
Both trigger and end signals have values lower than 1 and these are assigned from road surface information. Since stiffness factor is not very different between various surface conditions, the same trigger and end signals can be assigned and plugged into the algorithm, and decrease the dependency on surface conditions. For instance, the surface of the low slip road is indicated by dotted lines and has different formations than that of high mu roads, as shown in Figure 6. It is difficult to have individual starting points of the algorithm for the roads shown in line (b) and line (d), but normalized stiffness (b/a, d/c) will have similar values. That is why it is possible to use the same trigger and end signals. This is possible because the changes in stiffness can be observed in real-time using the stiffness based estimation method introduced in Section 3.3.

## 4. SIMULATION AND EXPERIMENTAL VALIDATION

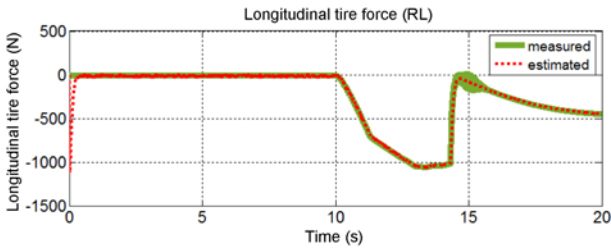
The performance of the estimator was simulated using Carsim and a compact size car on a dry asphalt road (SN/55). Various road surface conditions with Carsim and Simulink must be verified prior to the actual experiment. Experiments and then be conducted under conditions equal to that of the simulation environment.

### 4.1. Simulation Results

A hatchback vehicle was used for the simulation verification. First, the algorithm was verified under emergency braking conditions on a high mu road surface. Figure 7 shows the longitudinal tire force estimation (7) as it came to a stop from 70 km/h to 0. The estimated value was obtained by controlling the UIO gain values, which adequately collects tire force estimates in all ranges. The brake torque is induced by calculating the pressure at the master cylinder (9).

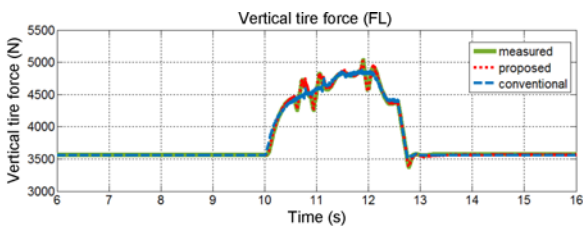


(a) Simulation: Longitudinal tire force estimation for front left tire

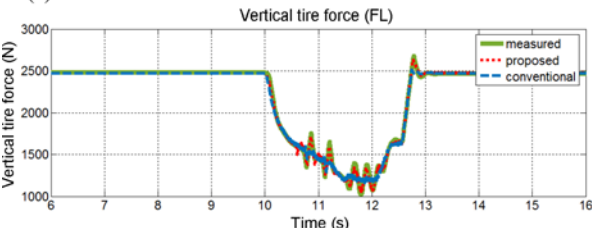


(b) Simulation: Longitudinal tire force estimation for rear left tire

Figure 7. Simulation of longitudinal tire force estimation.



(a) Simulation: Vertical tire force estimation for front left tire



(b) Simulation: Vertical tire force estimation for rear left tire

Figure 8. Simulation of vertical tire force estimation.

Figure 8. shows the tire force estimation when the suspension effect is taken into account or not. In the simulation, manmade disturbances were added to the road to simulate potholes and bumps. Currently used methods cannot track the tire force measurement ([10.5, 11.2], [11.8, 12.3] (s)). However, the proposed vertical tire force estimator takes the suspension effect into account and shows better performance in a wide spectrum.

Figure 9 shows that stiffness base estimation result from the normalizing the estimated tire force. The algorithm start to run for approximately 10 seconds of speed reduction, where the convergence value of 20 was recorded at low slip range (lower than 5 % tire slip). The estimated stiffness value coincided with the simulation environment, but it does have its limitations as mentioned previously.

Figure 10 (a) shows the simulation of advanced tire-road friction coefficient results. Figure 10 shows an increase of

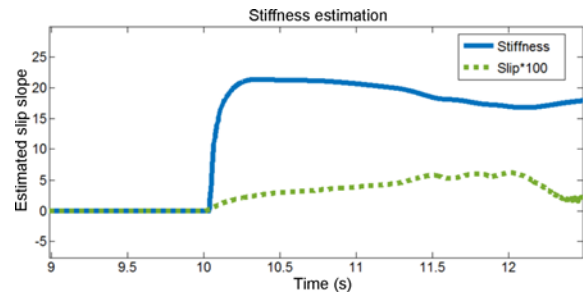
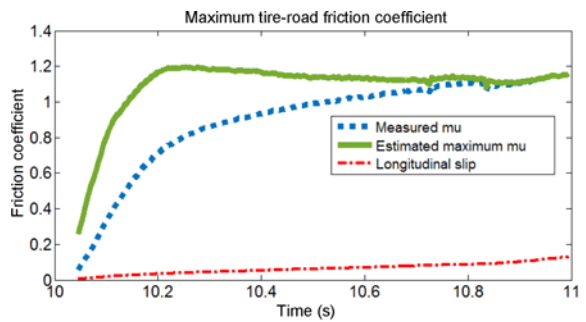
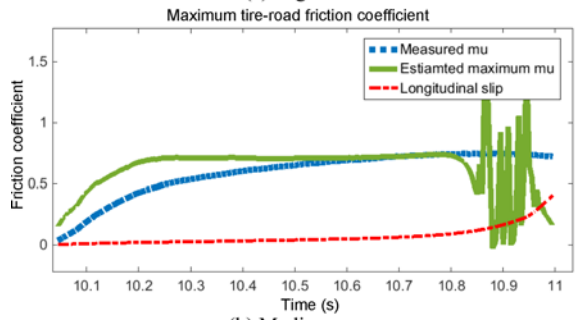


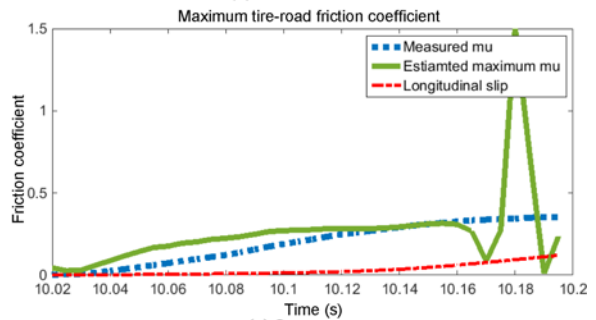
Figure 9. Simulation: Stiffness estimation.



(a) High mu



(b) Medium mu



(c) Low mu

Figure 10. Simulation: Maximum tire-road friction coefficient estimation using proposed algorithm.

tire slip approximately 10 seconds after the car begins to slow down. An accepted predetermined value of 1.2 in the simulation environment is within the range of maximum tire-road friction coefficient at 10.2 seconds. The real-time actual friction coefficient was approximately 0.8 at that time. This simulation result shows that maximum tire-road friction coefficient can be predicted when the current tire

utilize 60 ~ 70 % of their maximum capability. In other word, tire longitudinal grip margin detection is available when the actual tire stays in linear region. Various simulations, including Figures 10 (b) and (c) were conducted to test the robustness of algorithm against the many road surfaces. The maximum tire-road friction coefficient of Figure 10 (b) was accepted at 10.2 seconds to be the true value but the real-time surface friction coefficient was only 0.5 at that time. The estimated value increased at 10.82 seconds as the slip increased drastically because the friction was starting to saturate. The friction coefficient estimation has useless value after saturation and therefore it does not affect algorithm estimation. Figure 10 (c) shows the results of the low slip surface simulation, which are similar to the previous two road condition results. Therefore, it is possible to predict the maximum friction coefficient before it actually reaches the maximum value as surface slip increases.

#### 4.2. Experimental Setup

An actual experiment was conducted using a compact size car on dry asphalt condition (SN/55). This paper did not take road inclination and disturbances into consideration. Wheel force transducer (SWIFT) was attached to the rear and front left tires to measure tire force and moment. 6D-IMU sensors collected acceleration data 3 axis away from the center of mass. Figure 11 shows two evaluation tests (of full braking and rapid halt). A full braking test was conducted first to analyse the road surface conditions. Surface data, as shown in Figure 14, has many slip ratios beyond the saturation point. This is due to the ABS being intentionally altered for test purposes. Subsequently, data during rapid halt was collected to evaluate the proposed algorithm. The controlled vehicle slowed down to 0.8 g after reaching 70 km/h and the force and moment obtained

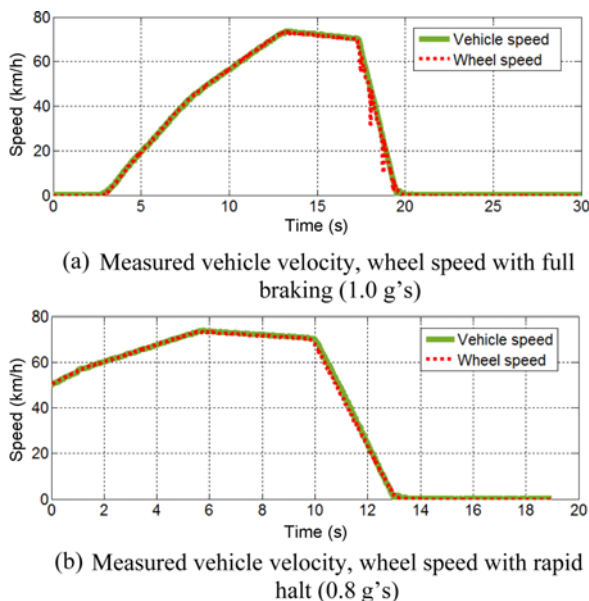


Figure 11. Simulation: Experiment: 70 km/h to 0 km/h.

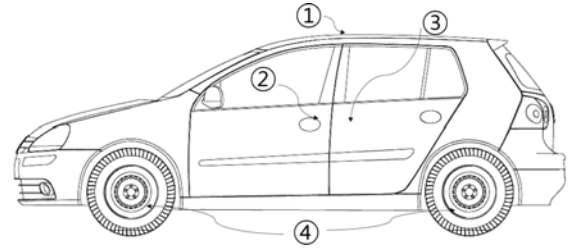


Figure 12. ① GPS receiver; ② 6D-IMU; ③ RT-3100; ④ SWIFT.

by a sampling frequency of 2 kHz was collected via Can Bus signal. Various data collected through 6D-IMU were filtered through the rate limiter to suppress single noises. During the moment of braking, the absolute speed and wheel speed differed, resulting in longitudinal slip. We obtained the wheel speed from wheel speed sensors and absolute vehicle speed from GPS. In the majority of passenger car, however, GPS signal is not available for cost issues. It also requires satellite based infrastructure, which may cause signal loss in specific environments such as urban, tunnel and forested region. We expect that this problem can be resolved for actual implementation using the proposed velocity estimation methods previously (You *et al.*, 2009; Oh and Choi, 2012). However, the development of highly accurate velocity observer is not our main focus in this paper so we simply used a GPS signal instead.

Figure 12 shows the used sensor position in this experimental. The test vehicle is equipped with a sensor that is suitable for verification of the proposed method.

The steering encoder and wheel speed sensor is readily available on the passenger car and we also use those signals. The additional sensors, GPS system and 6D-IMU, are also included to measure vehicle absolute speed, 3-axis accelerations, pitch, roll and yaw acceleration. The SWIFT sensor that measure tire force and moment, RT-3100 that measure highly accurate vehicle state estimation are used to measure reference value.

#### 4.3. Experiment Results

Figure 13 shows the estimated longitudinal and vertical tire force, which adheres to measured values from SWIFT. Slight vibrations seen in the measured values of the raw data were filtered using the rate limiter.

Figure 14 shows a graph of normalized force while the experimental car reduced speed to 1.0 g. Dots indicate normalized force raw data from SWIFT and line shows curve fitting results using raw data and the least squares method. Through these processes, we can safely conclude that the maximum tire-road friction coefficient has an approximate value of 1.0. However, the algorithm proposed in this paper shows a deterioration in estimation performance during full braking with experimental vehicles. This is because sufficient data is needed in the low slip range, but

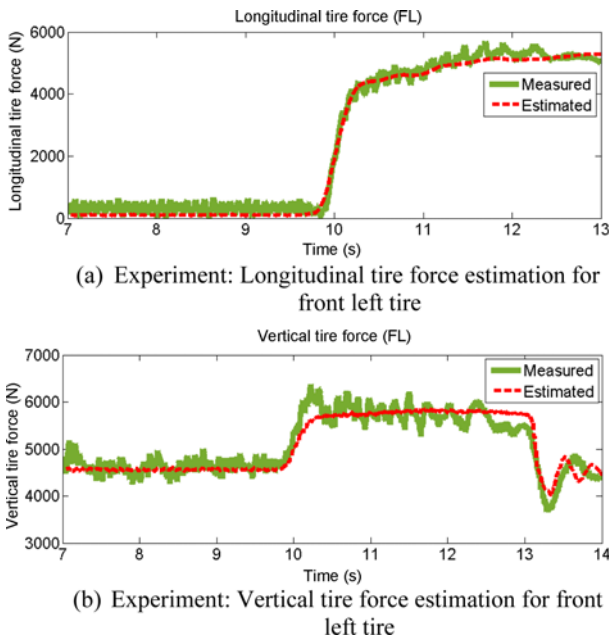


Figure 13. Simulation of tire force estimation.

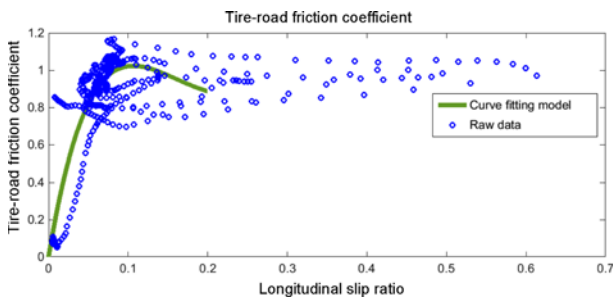


Figure 14. Normalized tire force versus slip ratio.

as shown in Figure 14, there is not enough normalized force data in this range during full braking. Therefore, additional braking experiments have been conducted to collect more data in the low slip range to test the algorithm.

The experimental evaluation of the proposed algorithm showed similar results to that of the simulation, as seen in Figures 15 and 16. Figure 15 is the result of estimating the

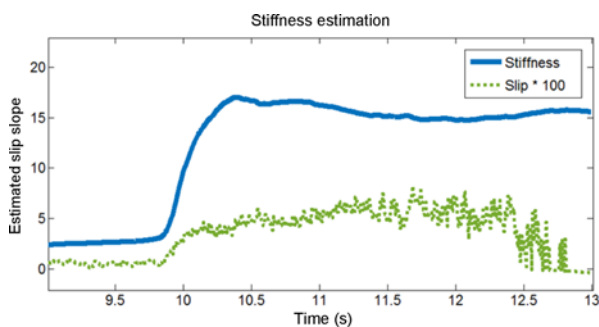


Figure 15. Experiment: Stiffness estimation.

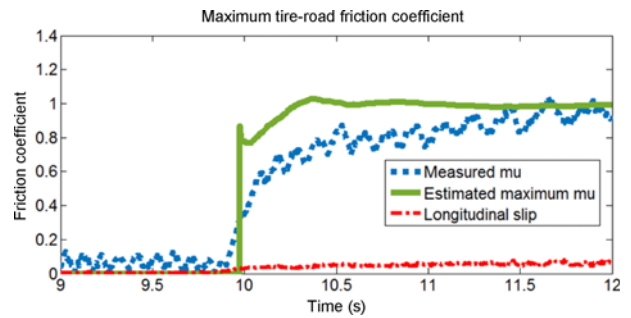


Figure 16. Experiment: Maximum tire-road friction coefficient estimation using a proposed algorithm.

inherent stiffness of the surface through the current stiffness based estimation method. It becomes the index for normalized stiffness factor.

The accepted tire-road friction coefficient from the SWIFT sensor measurements takes place at around 12 seconds, as shown in Figure 16. The estimated result of the algorithm was 10.3 seconds, very close to a true value of 1.0 and acceptable. Once again, it is possible to predict the maximum friction coefficient before the surface friction coefficient reaches its maximum. This information becomes very useful in predicting vehicle dynamic control.

#### 4.4. Algorithm Advantages and Limitations

A tire-road friction coefficient algorithm is already included in vehicle safety systems. However, the current automobile industry heavily relies on a rule based algorithm for safety reasons. That is why estimation of a robust friction coefficient is demanded, to reduce the sheer number of calculations.

The third order model was proposed under real-time curve fitting for the following reasons.

First, the reduction of calculations is possible due to the simple third order model. Second, estimation of peak slip range during maximum tire force, unlike current tire models in use, provides advantages. Finally, the maximum tire-road friction coefficient can be estimated via real-time curve fitting before longitudinal control takes over.

On the other hand, there are problems to the proposed algorithm which must be further studied. First, the lateral control system can be improved if an elliptical friction effect is considered including lateral dynamics. Moreover, if GPS systems can no longer provide the absolute speed of a vehicle, acceleration must be integrated to obtain absolute speed without causing a drifting effect. The proposed method also need an excitation signal input (PE condition) like previous works so if longitudinal slip does not exist, then estimation cannot be achieved. Finally, we must keep in mind that experimental evaluation of the algorithm was conducted on dry surface roads only. Although simulations using Carsim were performed under various road conditions, testing must be expanded to various non-experimental road surfaces for adoptability and robustness evaluation.

## 5. CONCLUSION

This paper proposed various methods of estimating maximum robust tire-road friction coefficient under irregular surface conditions. There have been many experiments in the past considering the use of an ideal mu-slip curve to estimate the friction coefficient. However, the mu-slip curve in real vehicle field tests shows many irregularities and other unforeseen factors, which affect curving phenomenon. This paper proposed an advanced tire-road friction coefficient algorithm with the aforementioned problems in mind. Various simulations and experiments were conducted using the suggested estimator. The new algorithm resolved previously mentioned problems and also reduced the amount of required calculation by introducing a third order model. Furthermore, factors that were previously difficult to measure, such as drive/brake torque, are now predictable using the algorithm. More tests are needed to evaluate the robustness of the algorithm as well as the including lateral friction coefficient in the future.

**ACKNOWLEDGEMENT**—This work was supported by the National Research Foundation of Korea (NRF) grant funded by the Korea government (MSIP) (No. 2010-0028680). This research was supported by the MSIP (Ministry of Science, ICT and Future Planning), Korea, under the C-ITRC (Convergence Information Technology Research Center) (IITP-2015-H8601-15-1005) supervised by the IITP (Institute for Information & communications Technology Promotion).

## REFERENCES

- Ahn, C., Peng, H. and Tseng, H. E. (2013). Robust estimation of road frictional coefficient. *IEEE Trans. Control Systems Technology* **21**, **1**, 1–13.
- Chen, W. and Saif, M. (2006). Unknown input observer design for a class of nonlinear systems: An LMI approach. *American Control Conf., IEEE*.
- Cho, W., Yoon, J., Yim, S., Koo, B. and Yi, K. (2010). Estimation of tire forces for application to vehicle stability control. *IEEE Trans. Vehicular Technology* **59**, **2**, 638–649.
- Choi, M. and Choi, S. (2014). Model predictive control for vehicle yaw stability with practical concerns. *IEEE Trans. Vehicular Technology* **63**, **8**, 3539–3548.
- Choi, M. and Choi, S. B. (2013). Estimation of four individual tire forces using limited sensor signals. *Int. J. Electrical Energy* **1**, **2**, 108–112.
- Choi, M., Oh, J. J. and Choi, S. B. (2013). Linearized recursive least squares methods for real-time identification of tire – Road friction coefficient. *IEEE Trans. Vehicular Technology* **62**, **7**, 2906–2918.
- Choi, S. B. (2008). Antilock brake system with a continuous wheel slip control to maximize the braking performance and the ride quality. *IEEE Trans. Control Systems Technology* **16**, **5**, 996–1003.
- Gustafsson, F. (1997). Slip-based tire-road friction estimation. *Automatica* **33**, **6**, 1087–1099.
- Gustafsson, F. (1998). Monitoring tire-road friction using the wheel slip. *Control Systems, IEEE* **18**, **4**, 42–49.
- Hahn, J.-O., Rajamani, R. and Alexander, L. (2002). GPS-based real-time identification of tire-road friction coefficient. *IEEE Trans. Control Systems Technology* **10**, **3**, 331–343.
- Han, K., Choi, S. and Oh, J. (2014). Estimation of vehicle clutch torque using combined sliding mode observers and unknown input observers. *Control, Automation and Systems (ICCAS), 14th Int. Conf., IEEE*, 1418–1423.
- Holzmann, F., Bellino, M., Siegart, R. and Bubb, H. (2006). Predictive estimation of the road-tire friction coefficient. *Computer Aided Control System Design, Int. Conf. Control Applications, Int. Symp. Intelligent Control, IEEE*, 885–890.
- Hori, Y., Toyoda, Y. and Tsuruoka, Y. (1998). Traction control of electric vehicle: Basic experimental results using the test EV “UOT electric march”. *IEEE Trans. Industry Applications* **34**, **5**, 1131–1138.
- Ito, M., Yoshioka, K. and Saji, T. (1995). Estimation of road surface conditions using wheel speed behavior. *JSAE Review*, **16**, 221–222.
- Kim, C., Hahn, J., Hong, K. and Yoo, W. (2013). Estimation of tire-road friction coefficient based on on-board 6-DoF acceleration measurement. *IEEE Trans. Vehicular Technology* **64**, **8**, 3368–3377.
- Kim, H., Lee, S. and Hedrick, J. (2015). Active yaw control for handling performance improvement by using traction force. *Int. J. Automotive Technology* **16**, **3**, 457–464.
- Lee, C., Hedrick, K. and Yi, K. (2004). Real-time slip-based estimation of maximum tire-road friction coefficient. *IEEE/ASME Trans. Mechatronics* **9**, **2**, 454–458.
- Lian, Y., Zhao, Y., Hu, L. and Tian, Y. (2015). Cornering stiffness and sideslip angle estimation based on simplified lateral dynamic models for four-in-wheel-motor-driven electric vehicles with lateral tire force information. *Int. J. Automotive Technology* **16**, **4**, 669–683.
- Muller, S., Uchanski, M. and Hedrick, K. (2003). Estimation of the maximum tire-road friction coefficient. *J. Dynamic Systems, Measurement, and Control* **125**, **4**, 607–617.
- Munson, B. R., Young, D. F. and Okiishi, T. H. (1990). *Fundamentals of Fluid Mechanics*. John Wiley & Sons. New York.
- Nam, K., Oh, S. and Hori, Y. (2010). Robust yaw stability control for electric vehicles based on active steering control. *Vehicle Power and Propulsion Conf. (VPPC), IEEE*, 1–5.
- Oh, J. J. and Choi, S. B. (2012). Vehicle velocity observer design using 6-d imu and multiple-observer approach. *IEEE Trans. Intelligent Transportation Systems* **13**, **4**, 1865–1879.
- Pacejka, H. (2005). *Tire and Vehicle Dynamics*. Elsevier. USA.

- Paleologu, C., Benesty, J. and Ciochina, S. (2008). A robust variable forgetting factor recursive least-squares algorithm for system identification. *Signal Processing Letters, IEEE*, **15**, 597–600.
- Rajamani, R. (2011). *Vehicle Dynamics and Control*. Springer Science & Business Media. New York.
- Rajamani, R., Phanomchoeng, G., Piyabongkarn, D. and Lew, J. Y. (2012). Algorithms for real-time estimation of individual wheel tire-road friction coefficients. *IEEE/ASME Trans. Mechatronics* **17**, **6**, 1183–1195.
- Ray, L. R. (1997). Nonlinear tire force estimation and road friction identification: simulation and experiments. *Automatica* **33**, **10**, 1819–1833.
- Sato, Y., Kobayashi, D., Watanabe, K., Watanabe, K., Kuriyagawa, Y. and Kuriyagawa, Y. (2007). Study on recognition method for road friction condition. *JSAE Trans.*, **38**, 51–56.
- Sierra, C., Tseng, E., Jain, A. and Peng, H. (2006). Cornering stiffness estimation based on vehicle lateral dynamics. *Vehicle System Dynamics*, **44**, 24–38.
- Wang, J., Alexander, L. and Rajamani, R. (2004). Friction estimation on highway vehicles using longitudinal measurements. *J. Dynamic Systems, Measurement, and Control* **126**, **2**, 265–275.
- Yoon, J., Cho, W., Koo, B. and Yi, K. (2009). Unified chassis control for rollover prevention and lateral stability. *IEEE Trans. Vehicular Technology* **58**, **2**, 596–609.
- You, S.-H., Hahn, J.-O. and Lee, H. (2009). New adaptive approaches to real-time estimation of vehicle sideslip angle. *Control Engineering Practice* **17**, **12**, 1367–1379.